Central European Journal of Energetic Materials
ISSN 1733-7178; e-ISSN 2353-1843

Cent. Eur. J. Energ. Mater. 2023, *20*(2): 114-137; DOI 10.22211/cejem/168343
Article is available in PDF-format, in colour, at:
https://ipo.lukasiewicz.gov.pl/wydawnictwa/cejem-woluminy/vol-20-nr-2/

Research paper

Thermal Decomposition of Ammonium Perchlorate Encapsulated with Copper(II)/Iron(III) Oxide Nanoparticles

Jelena D. Gržetić*[,1)], Slavko Mijatov[1)], Bojana Fidanovski[1)], Tihomir Kovačević[1)], Vladimir B. Pavlović[2)], Saša Brzić[1)], Danica Bajić[1)]

[1)] *Military Technical Institute, Belgrade, Serbia*

[2)] *University of Belgrade, Faculty of Agriculture, Belgrade, Serbia*

* *E-mail:* jrusmirovic@tmf.bg.ac.rs

ORCID information:
Gržetić J.D.: 0000-0002-7151-2666

Abstract: Thermal decomposition of ammonium perchlorate (AP), as a high energy oxidizer in composite solid rocket propellants (CSRP), greatly affects the burning rate of the propellant. This paper summarizes the results of a study of the synergistic catalytic activity of nano-CuO/Fe_2O_3 nanoparticles on thermal decomposition of AP. AP micro-particles are efficiently encapsulated with 1 and 5 wt.% of nano-CuO and/or nano-Fe_2O_3 nanoparticles by the fast-crash solvent-antisolvent technique. The efficiency of the encapsulation method was confirmed using FT-IR spectroscopy. Morphological characterization, performed using SEM-EDS microscopy, showed that encapsulation provides recrystallization and deagglomeration of AP and uniform nano-catalyst distribution. The catalytic efficiency of nano-CuO/ nano-Fe_2O_3 nanoparticles on the thermal decomposition of AP was investigated using DSC, and an increase in released heat was observed from 1453 to 1628 J/g. The catalytic activities of performed nano-catalysts were proven by decreasing the HTD and merging with the low decomposition temperature peak. The highest catalytic effect was obtained after encapsulating with 5 wt.% of nano-CuO and nano-Fe_2O_3 combined in a 50/50 mass ratio due to multiple mechanisms of catalytic activity of nano-Fe_2O_3. The effect of AP encapsulation

with nano-Fe_2O_3 on the burning rate of CSRP was investigated and the obtained results showed a favorable effect on the combustion rate law.

Keywords: energetic materials, propellant burning rate, nanoparticles, combustion, nano-catalysts

Nomenclature

AP	Ammonium perchlorate, NH_4ClO_4
CO	Castor oil
CSRP	Composite solid rocket propellants
DSC	Differential Scanning Calorimetry
DTG	Derivative Thermogravimetry
EDS	Energy dispersive X-ray technique
FSA	Fischer subsievesizer analyzer
FT-IR	Fourier-transform infrared spectroscopy
ΔH	Heat absorption
HTD	High temperature decomposition
HTPB	Hydroxyl-terminated polybutadiene
IPDI	Isophoronediisocyanate
LTD	Low temperature decomposition
m-AP	Modified micro-sized AP
m-CSRP	CSRP composition with micro-sized catalyst
n-CSRP	CSRP composition with nano-sized catalyst
nano-CuO	Nano-sized copper(II) oxide
nano-Fe_2O_3	Nano-sized iron(III) oxide
PSA	Particle Size Analyzer
SD	Stagnant decomposition
SEM	Scanning electron microscopy
R	Weight ratio between coarse and fine fraction of the AP
TET	Triethylenetetramine

1 Introduction

Cast-cured composite solid rocket propellants (CSRP) consist of an organic polymeric binder (hydroxyl-terminated polybutadiene, HTPB), a powdered metal as energetic fuel (aluminum or magnesium) and an inorganic oxidizer (ammonium perchlorate, AP). CSRPs also contain small concentrations of an antioxidant/stabilizer, curing and bonding agents, a plasticizer and a burning rate catalyst or depressant [1-3].

There are two approaches to deal with the demand for a high combustion rate and a high energy content:

(i) using oxidizers with smaller particle size (physical method) and

(ii) using ballistic modifiers (chemical method) to avoid complicated propellant grain design [4, 5].

It is known that the thermal decomposition of AP is specifically sensitive to the presence of certain additives, even in small amounts, which have a significant impact on the performance of rocket and missile systems [2, 6]. The most commonly used ballistic modifiers or burning rate catalysts are oxides of transition metal complexes (copper(II) oxide (CuO), iron(III) oxide (Fe_2O_3), strontium titanate, nickel(II) oxide, *etc.*) [4, 7-10]. The essence of their effect on the burning rate is the lowering of the thermal decomposition temperature of AP, because the higher the degradation temperature of the oxidizer, the lower the burning rate of the propellant. Nano-sized particles in CSRP formulations decrease the activation energy for oxidizer decomposition, which initiates combustion chemical reactions, giving a high energy release and resulting in increased burning rates [11, 12]. Propellant burning rate as well as temperature sensitivity are the basic ballistic characteristics of these energetic materials [13]. Vieille's Law (or St. Robert's Law) describes the linear burning rate, in the range of operating pressures equation (Equation 1):

$$r = a \cdot p^{n} \tag{1}$$

where r is the linear burning rate, which represents the rate of flame spreading normal to the combustion surface ($mm \cdot s^{-1}$), a is an empirical constant conditioned by the ambient temperature, p is the chamber combustion pressure (bar) and n is the pressure exponent, which is independent of temperature but describes the effect of pressure on the burning rate [14]. This equation can be used when the change in the pressure rate in the motor chamber is small enough and when the combustion pressure is approximately constant over the entire combustion surface. As n approaches the value of 1, the burning rate becomes very sensitive to small pressure changes. Low values of the pressure exponent in the combustion rate law are desirable [15, 16].

The temperature sensitivity of the propellant burning rate manifests through the combustion mechanism, *i.e.* the change in the propellant burning rate is proportional to the change in the propellant temperature (T_0) [3]. The temperature sensitivity of the burning rate should be as low as possible so that it does not significantly affect the values of pressure and thrust during the operation of the rocket motor in a wide range of temperature. Also, the burning rates of CSRPs are highly dependent on the initial propellant temperature [17]. Some recent papers

show that nano-sized particles of metal oxides, such as CuO, Fe_2O_3, MnO, NiO, PbO, TiO_2 could increase the burning rate of CSRPs [18-22]. The main role of metal oxides is to reduce the activation energy for oxidizer decomposition, which is high because that process is endothermic and results in the release of free oxygen. As the activation energy decreases, the required temperature for oxidizer decomposition is lowered, which provides the initiation of extremely exothermic combustion reactions and thus, higher burning rates of the propellant [22].

It is important to note that the appearance of agglomerates could be a problem in the case of the application of nanomaterials if the distribution of particles within the binder is not uniform [23]. However, some researchers, in order to avoid agglomeration, incorporate nano-sized Fe_2O_3 (nano-Fe_2O_3) onto graphene and its derivatives, so that the nanocomposites so formed exhibit improved catalytic performance for AP thermal decomposition [24]. Nano-sized materials show improved properties due to the substantial increase in active surface area [6]. Among them, nano-sized CuO (nano-CuO) is an ideal candidate for accelerating AP degradation due to its efficiency, low cost and high active surface [21].

The application of nanomaterials in the weapons industry and defence technologies is widespread throughout the world [25, 26]. A many publications on the application of different types of nanoparticles in the production of energetic materials are available in the scientific and professional literature [5, 8, 9, 13] De la Fuente *et al.* [27] deals with the development and characterization of propellant compositions with nano- and micro-sized CuO, in order to examine the impact on the burning rate of these materials. Yang *et al.* [28] state that nano-sized particles naturally represent a catalyst for the combustion of AP-based propellant compositions. In addition, the published results indicate a significant improvement in the inner-ballistic characteristics of the propellant, primarily the burning rate and the stability of the combustion process. The addition of 5% of nano-Fe_2O_3 to AP can considerably decrease its first and second thermal decomposition temperatures [29]. Fe_2O_3 can be used not only as a catalyst but also as a high-energy ingredient in AP-based CSRP compositions [7].

In this study, modification of micro-sized AP particles (m-AP) by encapsulation of nano-CuO and/or nano-Fe_2O_3 particles, using the fast-crash solvent-antisolvent technique, was performed. After modification, the thermal and morphological properties of AP were investigated in relation to the composition and amount of metal oxides employed. In addition, the ballistic characteristics were recorded as the modification decreases the decomposition temperature of AP and increases the heat release during its degradation, which are two important criteria for evaluating the performance of solid propellants [24].

2 Material and Methods

2.1 Materials

AP (grade IZ-200-TCP), procured from Eruca Technologies (Czech Republic), has been used as an oxidizer in CSRP compositions. A bimodal AP mixture, 10 and 200 μm average particle size, has been chosen to increase the oxidizer loading and propellant efficiency. The oxidizer was dried at 60 °C for 5 days to remove moisture before use. Commercial grade HTPB (mean molar mass 2900 $g \cdot mol^{-1}$, functionality 2.4) was obtained from Sartomer (USA). nano-CuO and nano-Fe_2O_3 catalysts with average particle size of 200 nm, 2-propanone and dichloromethane were procured from Sigma Aldrich. Castor oil (CO) from Interhem Ltd. (Serbia), with average molar mass 933 $g \cdot mol^{-1}$ and functionality 3.0, was used as plasticizer and bonding agent. Other compounds in the CSRP compositions are:

- 2,2'-methylene*bis*(4-methyl-6-*tert*-butylphenol) as antioxidant (AO 2246, Irganox),
- alumina with average particle size of 15 and 30 μm (X-71 and X-86, Alcan Toyo),
- triethylenetetramine (TET, Reidl) as bonding agent, and
- isophoronediisocyanate (IPDI, Evonik) as curing agent (Acros Organics, Germany).

2.2 Preparation of ammonium perchlorate powder encapsulated with nano-CuO and nano-Fe_2O_3 nanoparticles

The fine AP fraction (~10 μm) was obtained by grinding coarse AP (200 μm) using an ACM-10 hammer mill. The resulting fraction was dried at 70 °C for 48 h, and then characterized and subjected to additional modification. Prior to AP modification, nano-CuO and/or nano-Fe_2O_3, were dispersed in acetone using a magnetic stirrer, and then AP was dissolved in the obtained dispersion. The mass ratio of AP to nanoparticles was adjusted to 95:5 and 99:1. AP microparticles were encapsulated with CuO by the fast-crash solvent-antisolvent technique, where dichloromethane was used as an antisolvent. Precipitated particles of encapsulated AP were filtered and dried in a vacuum oven at 70 °C. Figure 1 shows a schematic illustration of the fast-crash solvent-anti solvent process for AP.

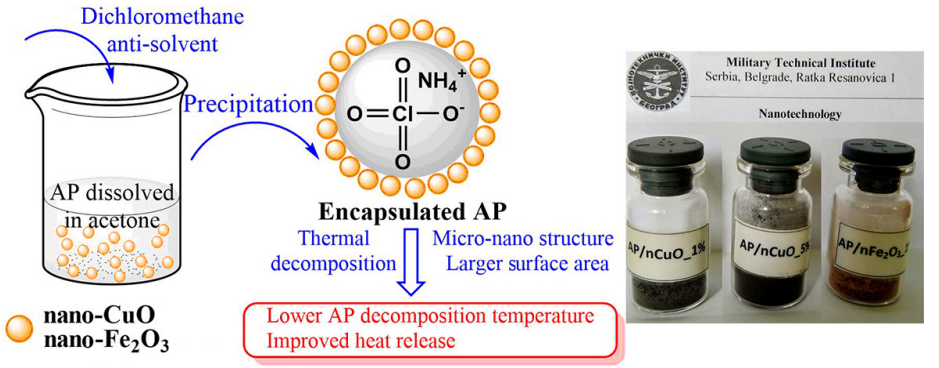

Figure 1. A schematic illustration of a fast-crash solvent-anti solvent process for AP encapsulation with nano-CuO and nano-Fe_2O_3

2.3 Characterization methods

Particle size distribution and average particle size of nano-CuO and nano-Fe_2O_3 were determined utilizing Particle Size Analyzer (PSA 1190 L/D, Anton Paar) in liquid operation mode by dispersing the powders using an ultrasonic unit within the device. The average diameter of coarse AP particles was determined using a Fischer subsievesizer analyzer HMK-22 (FSA). Powdered AP (1.95 g) was placed in a compression tube and the average size was determined by changing the compression level to a critical value depending on its density.

Analysis of the nano-CuO and nano-Fe_2O_3 distribution after AP encapsulation was performed using an SMTV Visor Inspection System (Michael Bruch, Germany). Furthermore, the morphology, size and shape of the modified AP particles were investigated using scanning electron microscopy (SEM) and energy dispersive X-ray technique (EDS). Samples were first coated with gold for 100 s at 30 mA, on a Baletic device SCD 005 Sputter coated. The SEM micrographs were recorded using a JEOL JSM-639LV SEM microscope, coupled with an electron dispersive spectroscope (EDS, Oxford Instruments, X-MaxN).

Fourier-transform infrared spectroscopy (FT-IR) curves of the encapsulated AP were recorded in absorbance mode using a Nicolet™ iS™ 10 FTIR spectrophotometer (Thermo Fisher Scientific, Waltham, Massachusetts, United States) with Smart iTR™ attenuated total reflectance (ATR) sampling accessories, within a range of 400-4000 cm^{-1}, at a resolution of 4 cm^{-1} and in 20 scan modes.

The total heat release upon complete decomposition of the oxidizer was determined using a DSC device (DSC Q20, TA, USA). The tested samples were heated from 60 to 480 °C at a heating rate of 5 °C·min^{-1} under a constant nitrogen flow rate of 50 $cm^3 \cdot min^{-1}$.

The mechanical characteristics of aluminized CSRP were determined using standard tensile tests performed using an Instron 1122 Universal Testing Instrument at 20 °C with a force loading rate of 50 mm·min^{-1}. The tensile properties were determined using seven standard JANNAF C specimens (dog-bone shape). The average value is presented.

3 Results and Discussion

3.1 Particle size analysis and morphological characterization of raw materials: AP and nano-CuO/nano-Fe_2O_3

The results obtained from the FSA device indicate that the average diameter of the ground AP particles is 10 μm, which is the optimal size for AP-bimodal CSRP formulations where 200 μm AP is used as the coarse fraction [30, 31]. Such a distribution of the AP size (200/10 μm) in bimodal mixtures provides the optimal particle packing/composition in HTPB binder [30]. The particle size distribution and average particle size of the nano-CuO and nano-Fe_2O_3, obtained by PSA technique, are shown in Figure 2.

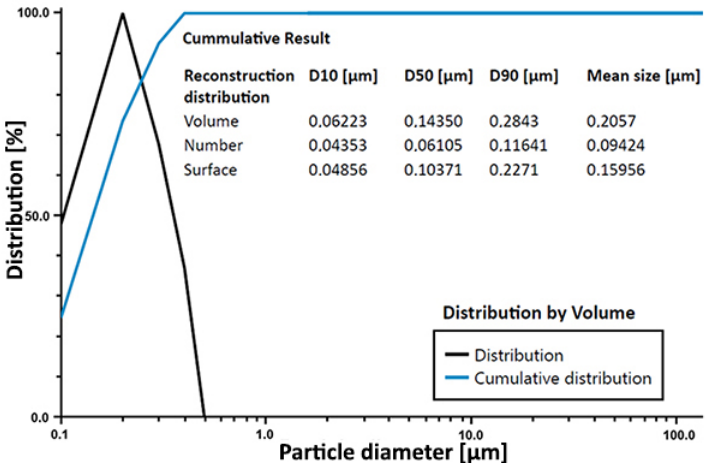

(a)

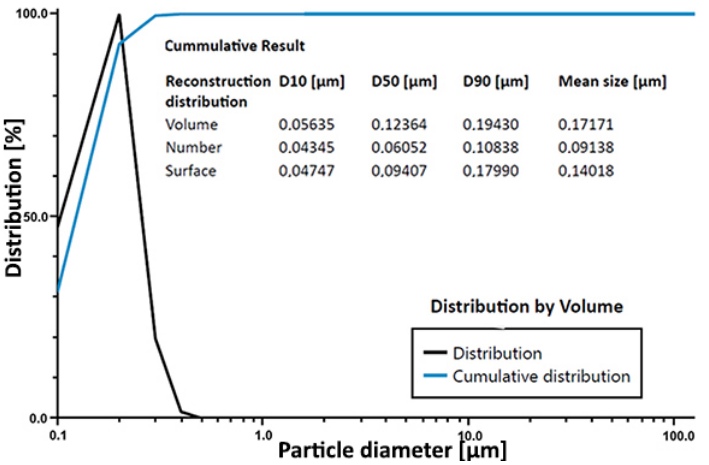

(b)

Figure 2. Particle size distribution of nano-CuO (a) and nano-Fe_2O_3 (b)

Figure 2 shows that the particles are successfully dispersed, no agglomerates remain and there is one sharp peak at approximately 100 nm. The values for D10, D50 and D90, as well as the average size, are given in Table 1.

Table 1. PSA results for nano-CuO and nano-Fe_2O_3 particles

Distribution	D10 [µm]	D50 [µm]	D90 [µm]	Average size [µm]
Volume	0.062	0.144	0.284	0.206
Volume	0.056	0.124	0.194	0.172

SEM images of nano-CuO and nano-Fe_2O_3 are given in Figure 3 (magnification of 10,000x, 25,000x and 40,000x), confirm the results obtained by PSA analysis regarding the approximate particle size of the modifiers. In addition, it can also be remarked from Figure 3 that these particles are, to some extent, organized into agglomerates of various sizes.

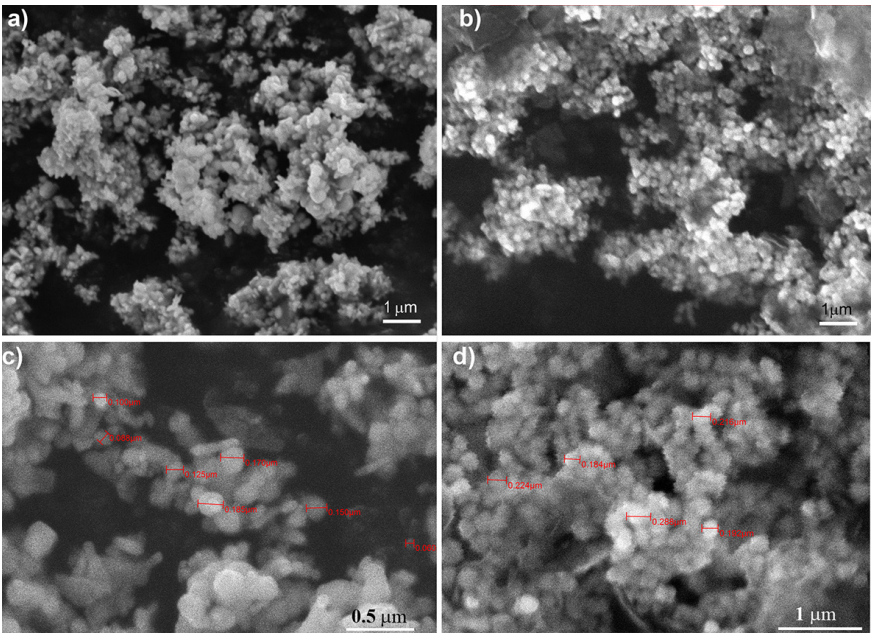

Figure 3. SEM micrographs of nano-CuO at 10,000x (a), nano-Fe_2O_3 at 10,000x (b), nano-CuO at 40,000x (c) and nano-Fe_2O_3 at 25,000x (d)

3.2 Morphological characterization of encapsulated AP

Optical microscopy was used as for an initial step in the surface characterization of pristine as well as modified AP particles (Figure 4). Figure 4 shows a uniform nanoparticle distribution on the AP surfaces, especially when the amount of inorganic oxides is 5 wt.% (Figures 4(b) and 4(d)). Some clustering can be seen when the amount of nanoparticles is 1 wt.% and this phenomenon being more pronounced in the case of nano-Fe_2O_3 (Figure 4(c)). The recrystallization process, which occurs during the encapsulation process, is fast and ensures breaking of the formed lumps resulting in uniformly coated/encapsulated AP crystals. Conversely, vacuum drying of the precipitated/recrystallized AP particles coated with nano-CuO/nano-Fe_2O_3 tends to create an insignificant number of AP clusters of higher dimensions (Figure 4(c)).

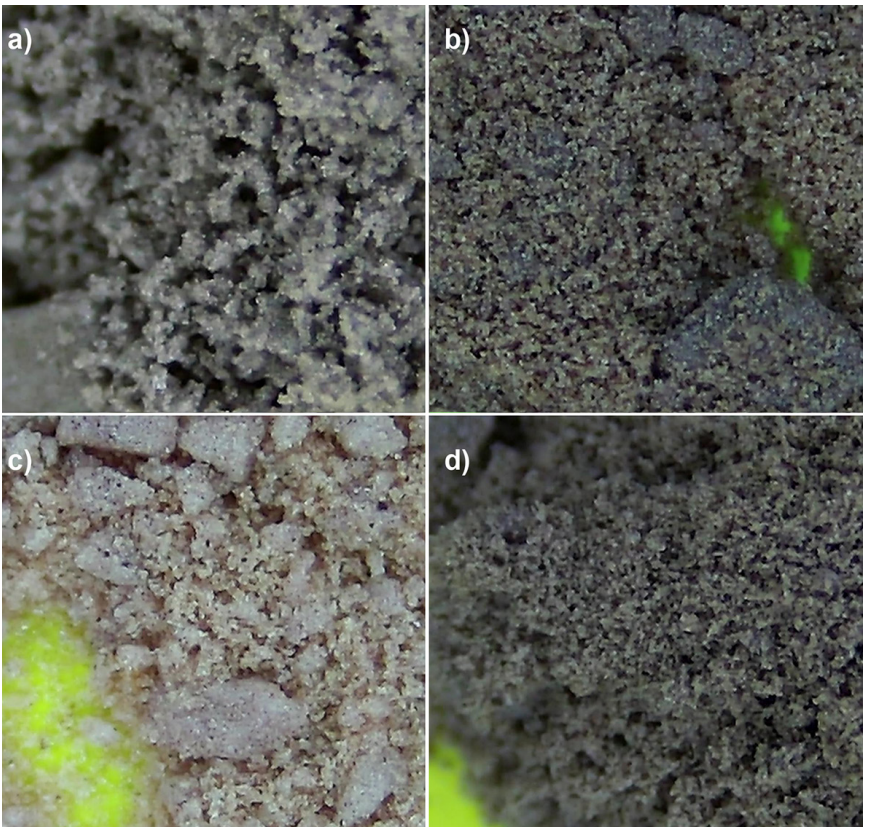

Figure 4. Optical images of AP coated with nano-CuO (99:1) (a), nano-CuO (95:5) (b), nano-Fe_2O_3 (99:1) (c) and nano-CuO/nano-Fe_2O_3 = 50/50 (95:5) (d)

Furthermore, the morphology of AP particles before and after coating was analyzed from SEM micrographs (Figure 5). Pristine AP grains have smooth surfaces, irregular shapes and crystalline domains with sharp edges (Figure 5(a)) [32]. The particle diameters are in the range of 4.40 to 12.01 μm, with myriad agglomerates of 34.26 μm. The introduction of nano-CuO nanoparticles onto AP surfaces is clearly evident in Figure 5(b). The modification process, which involves adhering of metal oxides on AP surfaces, significantly reduces the size and number of agglomerates. In addition, the nano-CuO layer prevents direct contact of AP particles, reducing their interaction and thus inhibiting the establishment of agglomerates (Figure 5(b)).

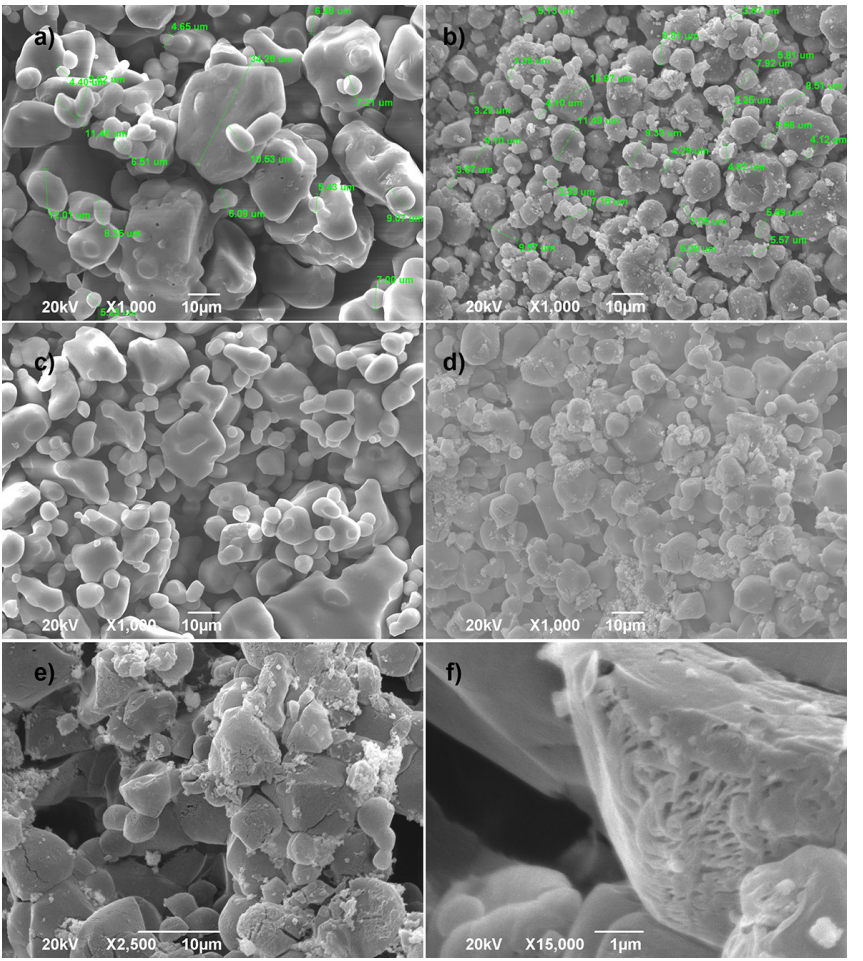

Figure 5. SEM micrographs of pristine AP (a), AP encapsulated with nano-CuO (95:5) (b), pristine AP treated at 190 °C (c), AP encapsulated with nano-CuO (95:5) treated at 190 °C at: 1,000, 2,500 and 15,000× magnification (d)-(f), respectively

SEM analysis was also used to examine the thermal degradation of AP. Pristine and encapsulated AP particles were subjected to heat treatment at 190 °C under vacuum conditions and the results obtained are shown in Figures 5(c) and 5(d). Thermal treatment has negligible impact on pristine AP particles, since they retain a smooth surface, which indicates that the applied temperature is significantly below the thermal decomposition temperature of AP. Still, it can be clearly seen that there is a decrease in size of agglomerates upon heating,

primarily due to evaporation of moisture, which holds the powder particles together. Contrary to this, thermally treated modified AP particles display rough surfaces with numerous pores which cover the entire particle surface [33]. Such phenomena indicate the lowering of the degradation temperature of AP, induced by the catalytic effect of nano-CuO particles. This is evident in Figure 5(f), where myriad fissures confirm the occurrence of the degradation process, *i.e*. the release of easily volatile substances, which causes deterioration in the structure of the material. This phenomenon is thoroughly analyzed using DSC spectroscopy.

In addition, SEM analysis combined with EDS analysis, was used to confirm the success of the applied method for AP encapsulation. EDS analysis confirms the presence of ≈5% nano-CuO on the AP surface. Also, the elements of AP present in the structure (N, Cl and O) were detected. A graphical representation of the elemental map obtained by EDS analysis is shown in Figure 6. After temperature treatment at 190 °C, the atomic weight % of Cu at surface increased to ≈8% due to moisture release and surface degradation.

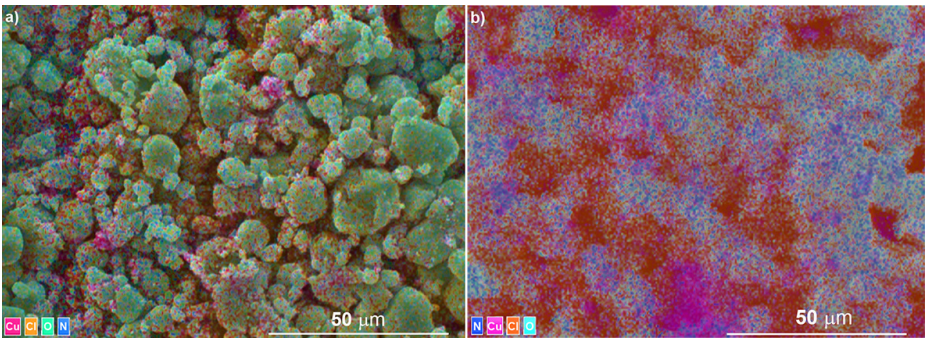

Figure 6. EDS analysis of a) AP coated with nano-CuO (95:5) and b) AP encapsulated with nano-CuO (95:5) treated at 190 °C

3.3 FT-IR results

FT-IR was used to qualitatively describe the encapsulation efficiency of AP with nano-CuO and nano-Fe_2O_3. FT-IR spectra, given in Figure 7, display the N–H and Cl–O asymmetric stretching and bending vibrations at 3270 and 1410 cm^{-1} as well as 1040 and 620 cm^{-1}, which originate to $–NH_4^+$ and $–ClO_4^-$, respectively [34]. Also, there is a band at 930 cm^{-1} that confirms the presence of stretching vibrations of Cl^- ions [35]. There is a characteristic peak for stretching vibrations of Cu–O at around 550 cm^{-1} (Figure 7(a)) [35]. The successful introduction of Fe_2O_3 onto the AP surfaces is confirmed by the peak at around 475 cm^{-1}, which is associated to the stretching vibrations of Fe–O [36, 37].

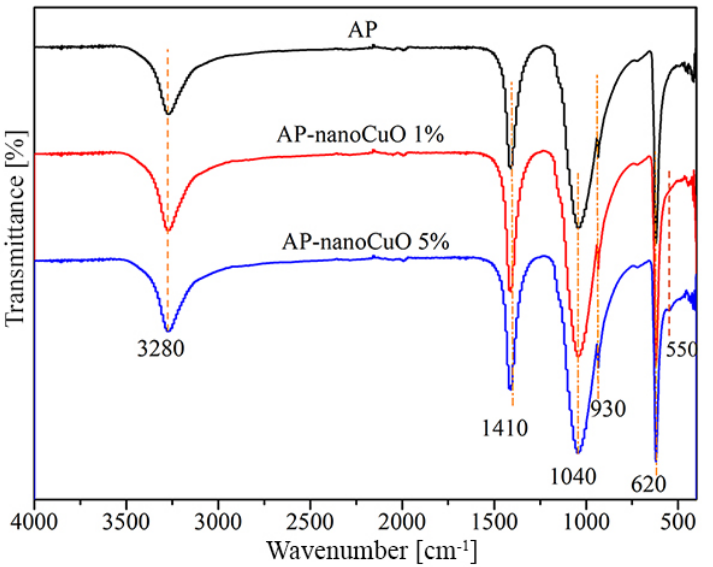

(a)

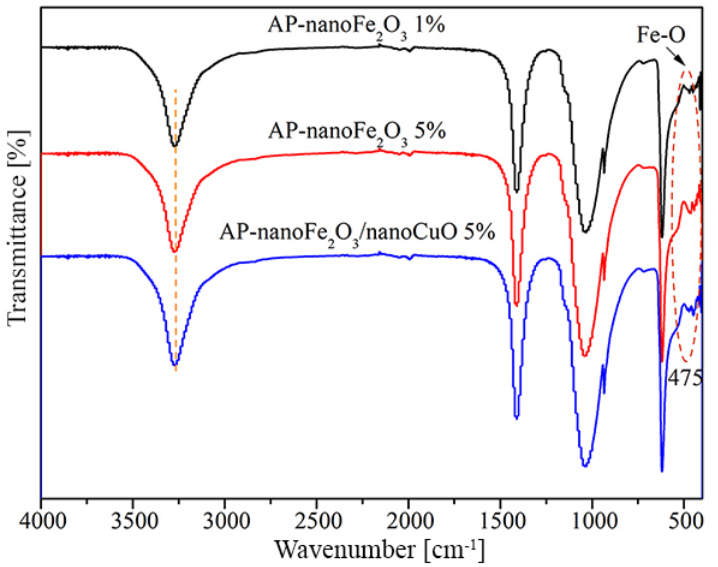

(b)

Figure 7. FT-IR spectra of pristine AP, AP encapsulated with 1 and 5 wt.% of nano-CuO (a) and AP encapsulated with 1 and 5 wt.% of nano-Fe_2O_3 and 5 wt.% of nano-CuO/nano-Fe_2O_3 = 50/50 (b)

3.4 Catalytic activity measurements

The decomposition of AP strongly depends on the experimental conditions, the presence of catalyst, the particle size of the catalyst and the method applied for AP modification [19]. DSC and DTG methods are commonly used for the understanding of thermal degradation processes and reaction paths that occur during the thermal treatment [38]. The efficiency of the fast-crash solvent-antisolvent technique (where AP oxidizer was coated with two different nano-CuO and nano-Fe_2O_3 amounts) was investigated using DSC analysis. Moreover, DSC analysis was used to investigate nanoparticle catalytic activity on the AP thermal degradation.

Thermal decomposition of pure AP takes place in two main stages: endothermic and exothermic [2, 24, 39], according to Figure 8(a). The first stage is the initial endothermic transition of AP from the orthorhombic to the cubic phase at 243.58 °C (this temperature is termed the low temperature decomposition (LTD)) [40]. This decomposition is accompanied with heat absorption of 176.10 $J \cdot g^{-1}$ (ΔH). The exothermic stage of AP decomposition includes two steps, degradation at 302.5 °C, with the formation of intermediate gaseous products such as ammonia (NH_3) and perchloric acid ($HClO_4$) through incomplete dissociation and sublimation (proton transfer from ammonium ions (NH_4^+) to perchlorate ions (ClO_4^-) in dehydrogenation and hydrogenation reactions) [41]. This step is accompanied with a heat release of 191.0 $J \cdot g^{-1}$. The second exothermic step occurs at 442.3 °C (this temperature is termed the high temperature decomposition (HTD)). During transition from the first to second exothermic step stagnation occurred, followed with NH_3 adsorption onto AP surface (stagnant decomposition (SD)). Complete decomposition of AP generates several low-molecular weight volatile molecules, such as ClO_2^-, ClO_3^-, ClO_2, HCl, H_2O, N_2O, Cl_2, NO, O_2, and NO_2, as a result of total decomposition/oxidation of NH_3 and $HClO_4$ [40, 42].

Nano-CuO demonstrates a high catalytic activity for the thermal decomposition of AP, which is manifested through a decrease in the energy needed for degradation. Higher oxide concentration exhibits a slightly greater impact (Figures 8(b) and 8(c)) on the energy of the AP decomposition, from 176.10 to 91.28 and 88.44 $J \cdot g^{-1}$, respectively. This indicates that less energy is needed for the decomposition of the AP particles [22]. The ΔH decreases due to lowering of the activation energy necessary for the phase transition of AP particles. The subsequent two exothermic decomposition peaks almost merged into a broad one with total heat release of 1628 and 1527 $J \cdot g^{-1}$, Figures 8(b) and 8(c), respectively [22].

The main scientific contribution of this study is closely related with decreasing the HTD of AP and merging the main two exothermic decomposition

peaks into one (Figures 8(b)-8(d)) after encapsulation with nano-CuO and nano-Fe_2O_3 particles. This catalytic mechanism is accompanied by the adsorption of NH_3 onto the catalysts, which indicates a decrease in the accumulation/adsorption of NH_3 on the AP surface. The highest catalytic effect is obtained with 5 wt.% of an equal weight mixture of nano-CuO and nano-Fe_2O_3 (Figure 8(d)), which is caused by the multiple mechanism of the catalytic activity of nano-Fe_2O_3. Furthermore, the synergetic effects of these two oxides also come into play, which more efficiently prevents the deposition of ammonia on the AP surface. During the thermal decomposition of AP-nano-Fe_2O_3/nano-CuO 5 wt.% the adsorption of the NH_3 on both catalysts is supported by the formation of unstable intermediate compounds (iron and/or nitryl perchlorate) [19].

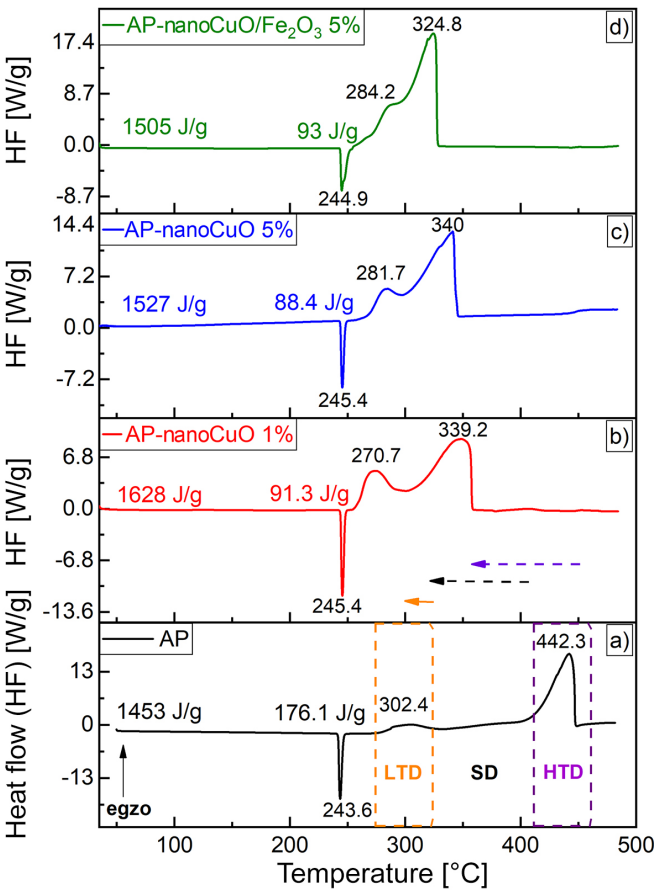

Figure 8. DSC thermographs for pristine AP (a), AP-nano-CuO 1 wt.% (b), AP-nano-CuO 5 wt.% (c) and nano-CuO/nano-Fe_2O_3 5 wt.% (50/50) (d)

A brief overview of the catalytic activity of various micro/nano transition metal oxides on the thermal decomposition of AP is tabulated in Table 2. Mahinroosta [39] reported a decrease in the HTD temperature when the mass ratio of AP/catalyst was 99/1 (Fe_2O_3) and 99/1 or 97/3 (CuO). Joshi *et al.* [19] also showed an HTD decrease when a metal oxide is used, but the effect was more moderate since the AP/catalyst ratio was lower (99.5/0.5). A significantly higher catalytic activity, *e.g.* a decrease in HTD, was reached when the AP/CuO mass ratio was 100/3 or when CuO nanoparticles were combined with NiO [21, 43]. Table 2 shows a comparative analysis of HTD obtained in previous studies and those from this paper. It can be seen that the combination of CuO and Fe_2O_3 in equal amounts results in a high catalytic activity for the decomposition of AP. Additionally, encapsulation of AP particles via the fast-crash solvent-antisolvent technique provides recrystallisation and deagglomeration of AP and uniform nano-catalyst distribution on the surface of AP. Finally, it possesses more active catalyst sites suitable for adsorption of the AP decomposition products (NH_3) and proton transfer. Such results confirm a promising applicability of nano-CuO and/or nano-Fe_2O_3 as burning rate catalysts in AP-based CSRP formulations.

Table 2. Literature reported data of catalytic activity of various micro/nano transition metal oxides on the thermal decomposition of AP

Catalyst	AP/Catalyst ratio	HTD peak [°C]	ΔH [$J \cdot g^{-1}$]	Ref.
Without catalyst	100/0	442.3	1453	This work
Fe_2O_3, commercial	99/1	403.6	n.p.	[39]
CuO, commercial	99/1	359.0	n.p.	[39]
	97/3	353.2	n.p.	[20]
Fe_2O_3, 3.5 nm size	99.5/0.5	425.0	1115	[19]
CuO nanocrystals	100/3	313.8	n.p.	[43]
NiO@CuO nanocomposite	98/2	310.0	1535	[21]
nano-CuO	99/1	339.2	1628	This work
	95/5	340.0	1527	This work
nano-CuO/nano-Fe_2O_3 (50/50)	95/5	324.8	1505	This work

3.5 Investigation of AP encapsulation with nano-Fe_2O_3 on propellant ballistic properties

Formulations of CSRP based on HTPB, shown in Table 3, were chosen for investigation. A bimodal mixture, consisting of particles with average particle sizes 200 and 10 μm, was used as an oxidizer.

Table 3. Examined compositions of CSRP

CSRP label	AP-200 [%]	AP-10 [%]	m-AP-10 [%]**	Al-15	Al-30	AP [%]	*R****	m-Fe_2O_3 [%]	Solid phase [%]	Prepolymer***** [%]
m-CSRP*	47.45	25.55	–	6.00	6.00	73	65/35	1.20	86.0	13.31
n-CSRP*		–	25.55					–		

* m-CSRP is CSRP composition with micro-sized catalyst, n-CSRP is CSRP composition with nano-sized catalyst;

** m-AP-10 – AP encapsulated with nano-Fe_2O_3 (1.20% of nano-Fe_2O_3 in final formulation);

*** *R* – weight ratio between coarse and fine fraction of the AP;

**** Prepolymer contains HTPB (11.28 wt.%) and CO (2.03 wt.%). The amount of curing agent, IPDI, was 1.16 wt.%

Propellant batches were homogenized at 60 °C in a laboratory vertical planetary mixer (4PU Baker Perkins, 4,8 l). Afterwards, the propellant slurry was cast in 2″ small-scale experimental motors for the ballistic examination at the experimental fire station by static testing [31]. After curing at an elevated temperature (T = 70 °C) for 120 h, inner-ballistic characterization was performed at 20 °C in the pressure range from 6 to 18 MPa by using four different nozzle sizes, 7.62, 8.11, 8.64 and 9.14 mm. The pressure exponent and burning rate were calculated from the burning rate law. Results of the examination of the inner-ballistic characteristics, as plots of pressure *vs*. time and burning rate *vs*. pressure, are presented in Figure 9.

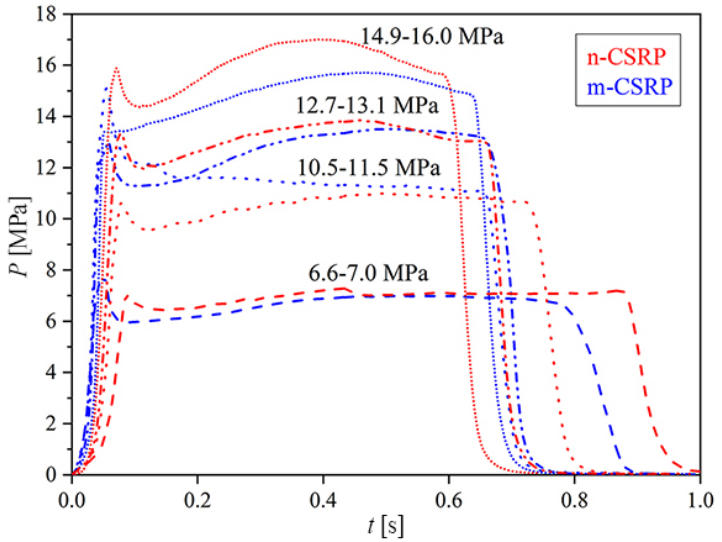

(a)

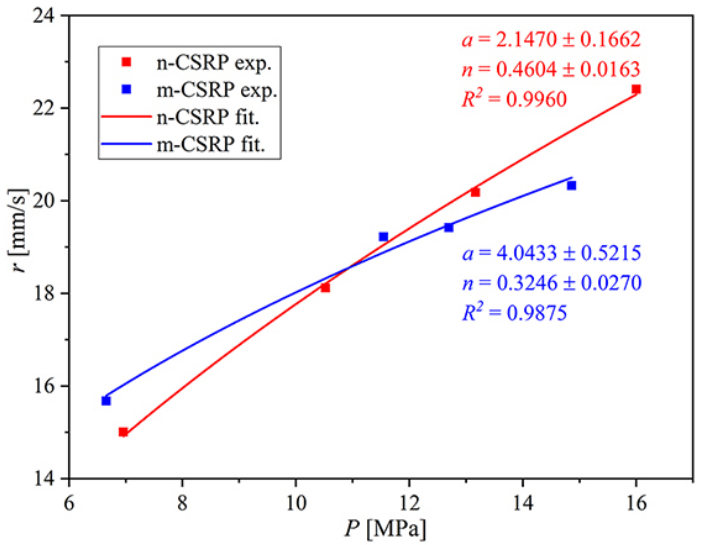

(b)

Figure 9. Inner-ballistic performances of m-CSRP and n-CSRP: pressure depending time combustion diagrams (a) and burning rate laws (b)

Prepared CSRP burning rates define the velocity of gas generation upon combustion, which further determine the pressure inside the rocket motor and the overall thrust. It is clear that combustion processes, in whole range of operating pressures, are stable for both m-CSRP and n-CSRP (Figure 9(a)).

The collected inner-ballistic experimental data were fitted using a burning rate law equation (Equation 1). This fitting should have a minimal distortion of the obtained shape of the burning rate curve in the defined range of operating pressures [16]. The pressure exponent of the m-CSRP formulation was 0.32 (6-15 MPa), which is lower than for n-CSRP (0.46; 6-16 MPa). The physical manifestation of the remarked phenomenon is the higher pressure as well as burning rate of the propellant containing the nano-scaled ballistic modifier (Figure 9(b)). This is attributed to its high active surface area, which accelerates the catalytic reactions and decreases the HTD temperature of the AP decomposition in the condensed-phase reaction zone at the beginning of the combustion process. In brief, this phenomenon during n-CSRP combustion triggers the endothermic decomposition of AP [22] earlier, which further initiates the highly exothermic combustion process, which leads to heat release and evolution of high temperature combustion products (more combustion products, higher motor chamber pressure). Such results are in correlation with the ones obtained from thermal DSC characterization. The obtained results indicate a high potential of application of n-CSRP in rocket systems, which require high operating pressures and burn rate, *e.g.* double-case designed solid rocket motor with booster.

The results for the mechanical properties of m-CSRP and n-CSRP showed a slight decrease in tensile strength, *e.g.* σ_t decreased from 0.58 to 0.34 MPa, while elongation at break (ε) increased from 67.0 to 92.0%, respectively, when micro-Fe_2O_3 was replaced with nano-Fe_2O_3. The main reason for such mechanical test results is potentially related to the appearance of agglomerates of the modified AP formed due to dipole-dipole bonding of surface nano-Fe_2O_3 which deteriorates the mechanical properties of the corresponding propellant. However, the mechanical characteristics obtained still remain within the required range for double-case or case-bonded solid rocket propellant ($\varepsilon \geq 30\%$). Such mechanical properties support stable combustion of the CSRP and justify the research of nano-energetic materials.

4 Conclusions

- Nanoparticles of copper(II)-oxide and iron(III)-oxide (nano-CuO and nano-Fe_2O_3) were successfully applied as ballistic modifiers of AP-based CSRPs.

They were used to encapsulate particles of AP using the fast-crash solvent-antisolvent technique.

- SEM micrographs of the encapsulated AP have revealed the quality of nanoparticle surface coating indicating that the employed technique provides recrystallization and de-agglomeration of oxidizer and uniform nano-catalyst distribution. The FT-IR technique confirmed the qualitative composition of the prepared samples prior to and after the AP encapsulation with nano-catalysts. Differential scanning calorimetry was used for evaluation of the catalytic efficiency of nano-CuO and/or nano-Fe_2O_3 on the AP thermal decomposition by detecting its initial degradation temperature.
- The highest catalytic effect was obtained after encapsulation with 5 wt.% of the equal weight mixture of nano-CuO and nano-Fe_2O_3 due to the multiple mechanism of catalytic activity of nano-Fe_2O_3.
- These results, achieved due to the unique catalyzing ability of nano-CuO and nano-Fe_2O_3, encourage future application of metal oxide catalysts in advanced energetic materials.

Acknowledgment

The authors acknowledge the support of this research from the Serbian Ministry of Education, Science and Technological Development (grant-contract No. 451-03-68/2022-14/200325).

References

[1] Yadav, N.; Srivastava, P.K.; Varma, M. Recent Advances in Catalytic Combustion of AP-based Composite Solid Propellants. *Def. Technol.* **2021**, *17*(3): 1013-1031; DOI: 10.1016/j.dt.2020.06.007.

[2] Singh, S.; Srivastava, P.; Singh, G. Nano Oxalates of Fe, Co, Ni: Burning Rate Modifiers for Composite Solid Propellants. *J. Ind. Eng. Chem.* **2015**, 27: 88-95; DOI: 10.1016/j.jiec.2014.11.047.

[3] Chalghoum, F.; Trache, D.; Benziane, M.; Benhammada, A. Effect of Micro- and Nano-CuO on the Thermal Decomposition Kinetics of High-performance Aluminized Composite Solid Propellants Containing Complex Metal Hydrides. *FirePhysChem* **2022**, *2*(1): 36-49; DOI: 10.1016/j.fpc.2022.03.007.

[4] Chen, T.; Hu, Y.-W.; Zhang, C.; Gao, Z.-J. Recent Progress on Transition Metal Oxides and Carbon-supported Transition Metal Oxides as Catalysts for Thermal Decomposition of Ammonium Perchlorate. *Def. Technol.* **2021**, *17*(4): 1471-1485; DOI: 10.1016/j.dt.2020.08.004.

[5] Suresh Babu, K.V.; Kanaka Raju, P.; Thomas, C.R.; Syed Hamed, A.; Ninan, K.N.

Studies on Composite Solid Propellant with tri-modal Ammonium Perchlorate Containing an Ultrafine Fraction. *Def. Technol.* **2017**, *13*(4): 239-245; DOI: 10.1016/j.dt.2017.06.001.

[6] Zhang, D.; Li, Q.; Li, R.; Li, H.; Gao, H.; Zhao, F.; Xiao, L.; Zhang, G.; Hao, G.; Jiang, W. Significantly Enhanced Thermal Decomposition of Mechanically Activated Ammonium Perchlorate Coupling with Nano Copper Chromite. *ACS Omega* **2021**, *6*(24): 16110-16118; DOI: 10.1021/acsomega.1c02002.

[7] Zhen, F.; Zhou, X.-Y.; Wang, L.-Q.; Yang, R.-J.; Huang, F.-L. Study on Burning and Thermal Decomposition Properties of HTPB Propellant Containing Synthesized Micro-nano Ferric Perfluorooctanoate. *Propellants Explos. Pyrotech.* **2019**, *44*(3): 362-368; DOI: 10.1002/prep.201800309.

[8] Rao, D.C.K.; Yadav, N.; Joshi, P.C. Cu–Co–O Nano-catalysts as a Burn Rate Modifier for Composite Solid Propellants. *Def. Technol.* **2016**, *12*: 297-304; DOI: 10.1016/j.dt.2016.01.001.

[9] Jain, S.; Gupta, G.; Kshirsagar, D.R.; Khire, V.H. Burning Rate and Other Characteristics of Strontium Titanate ($SrTiO_3$) Supplemented AP/HTPB/Al Composite Propellants. *Def. Technol.* **2019**, *15*: 3-8; DOI: 10.1016/j.dt.2018.10.004.

[10] Hu, Y.; Yang, S.; Tao, B.; Liu, X.; Lin, K.; Yang, Y.; Fan, R.; Xia, D.; Hao, D. Catalytic Decomposition of Ammonium Perchlorate on Hollow Mesoporous CuO Microspheres. *Vacuum* **2019**, *159*: 105-111; DOI: 10.1016/j.vacuum.2018.10.020.

[11] Yan, Q.-L.; Zhao, F.-Q.; Kuo, K.K.; Zhang, X.-H.; Zeman, S.; DeLuca, L.T. Catalytic Effects of Nano Additives on Decomposition and Combustion of RDX-, HMX-, and AP-based Energetic Compositions. *Prog. Energy Combust. Sci.* **2016**, *57*: 75-136; DOI: 10.1016/j.pecs.2016.08.002.

[12] Pang, W.-Q.; Fan, X.-Z.; Zhao, F.-Q.; Zhang, W.; Xu, H.-X.; Yu, H.-J.; Xie, W.-X.; Yan, N.; Liu, F.-L. Effects of Different Nano-Metric Particles on the Properties of Composite Solid Propellants. *Propellants Explos. Pyrotech.* **2014**, *39*(3): 329-336; DOI: 10.1002/prep.201300172.

[13] Atwood, A.I.; Boggs, T.L.; Curran, P.O.; Parr, T.P.; Hanson-Parr, D.M.; Price, C.F.; Wiknich, J. Burning Rate of Solid Propellant Ingredients. Part 1: Pressure and Initial Temperature Effects. *J. Propuls. Power* **1999**, *15*(6): 740-747; DOI: 10.2514/2.5522.

[14] Gupta, G.; Jawale, L.; Mehilal; Bhatacharya, B. Various Methods for the Determination of the Burning Rates of Solid Propellants – An Overview. *Cent. Eur. J. Energ. Mater.* **2015**, *12*(3): 593-620.

[15] Chaturvedi, S.; Dave, P.N. Solid Propellants: AP/HTPB Composite Propellants. *Arab. J. Chem.* **2019**, *12*(8): 2061-2068; DOI: 10.1016/j.arabjc.2014.12.033.

[16] Rodić, V.; Dimić, M.; Brzić, S.; Gligorijević, N. Cast Composite Solid Propellants with Different Combustion Stabilizers. *Sci. Tech. Rev.* **2016**, *65*(2): 3-10.

[17] Cohen-Nir, E. Temperature Sensitivity of the Burning Rate of Composite Solid Propellants. *Combust. Sci. Technol.* **1974**, *9*(5): 183-194; DOI: 10.1080/00102207408960356.

[18] Vara, J.A.; Dave, P.N.; Chaturvedi, S. The Catalytic Activity of Transition Metal

Oxide Nanoparticles on Thermal Decomposition of Ammonium Perchlorate. *Def. Technol.* **2019**, *15*(4): 629-635.

[19] Joshi, S.S.; Patil, P.R.; Krishnamurthy, V.N. Thermal Decomposition of Ammonium Perchlorate in the Presence of Nanosized Ferric Oxide. *Def. Sci. J.* **2008**, *58*(6): 721-727; DOI: 10.14429/dsj.58.1699.

[20] Alizadeh-Gheshlaghi, E.; Shaabani, B.; Khodayari, A.; Azizan-Kalandaragh, Y.; Rahimi, R. Investigation of the Catalytic Activity of Nano-sized CuO, Co_3O_4 and $CuCo_2O_4$ Powders on Thermal Decomposition of Ammonium Perchlorate. *Powder Technol.* **2012**, *217*: 330-339; DOI: 10.1016/j.powtec.2011.10.045.

[21] Juibari, N.M.; Tarighi, S. Metal-Organic Framework-derived Nanocomposite Metal-oxides with Enhanced Catalytic Performance in Thermal Decomposition of Ammonium Perchlorate. *J. Alloys Compd.* **2020**, *832*: paper 154837; DOI: 10.1016/j.jallcom.2020.154837.

[22] Elbasuney, S.; Yehia, M. Thermal Decomposition of Ammonium Perchlorate Catalyzed with CuO Nanoparticles. *Def. Technol.* **2019**, *15*(6): 868-874; DOI: 10.1016/j.dt.2019.03.004.

[23] Reid, D.L.; Draper, R.; Richardson, D.; Demko, A.; Allen, T.; Petersen, E.L.; Seal, S. *In situ* Synthesis of Polyurethane-TiO_2 Nanocomposite and Performance in Solid Propellants. *J. Mater. Chem. A* **2014**, *2*(7): 2313-2322; DOI: 10.1039/C3TA14027J.

[24] Chen, J.; He, S.; Liu, Y.; Qiao, Z.; Huang, B.; Li, X.; Hao, Q.; Huang, H.; Yang, G. Highly Active Catalysts Based on 3D Hierarchically Ordered Porous Carbon with Entrapped Fe_2O_3 Nanoparticles for the Thermal Decomposition of Ammonium Perchlorate. *Appl. Surf. Sci.* **2021**, *538*: paper 148148; DOI: 10.1016/j.apsusc.2020.148148.

[25] Simić, D.; Marjanović, M.; Vitorović-Todorović, M.; Bauk, S.; Lazić, D.; Samolov, A.; Ristović, N. Nanotechnology for Military Applications – A Survey of Recent Research in Military Technical Institute. *Sci. Tech. Rev.* **2018**, *68*(1): 59-72.

[26] Altmann, J. *Military Nanotechnology-Potential Applications and Preventive Arms Control.* Taylor & Francis Group, CRC Press, Canada, **2006**; ISBN 9780415407991.

[27] de la Fuente, J.L.; Mosquera, G.; Paris, R. High Performance HTPB-Based Energetic Nanomaterial with CuO Nanoparticles. *J. Nanosci. Nanotechnol.* **2009**, *9*(12): 6851-6857; DOI: 10.1166/jnn.2009.1579.

[28] Yang, Y.; Yu, X.; Wang, J.; Wang, Y. Effect of the Dispersibility of Nano-CuO Catalyst on Heat Releasing of AP/HTPB Propellant. *J. Nanomater.* **2011**: paper 180896; DOI: 10.1155/2011/180896

[29] Pang, W.; DeLuca, L.T.; Fan, X.; Maggi, F.; Xu, H.; Xie, W.; Shi, X. Effects of Different Nano-Sized Metal Oxide Catalysts on the Properties of Composite Solid Propellants. *Combust Sci Technol.* **2016**, *188*: 315-328; DOI: 10.1080/00102202.2015.1083986.

[30] Rodić, V.; Bajlovski, M. Influence of Trimodal Fraction Mixture of Ammonium-Perchlorate on Characteristics of Composite Rocket Propellants. *Sci. Tech. Rev.* **2006**, *56*(2): 38-44.

[31] Rodić, V.; Bogosavljević, M.; Milojković, A.; Mijatov, S. Preliminary Research of Composite Rocket Propellants with Hexogen and Titanium Oxide Powder. *Sci. Tech. Rev.* **2018**, *68*(2): 36-47.

[32] Liu, W.; Xie, Y.; Xie, Q.; Fang, K.; Zhang, X.; Chen, H. Dropwise Cooling Crystallization of Ammonium Perchlorate in Gas-Liquid Two-phase Suspension Systems. *RSC Chem. CrystEngComm.* **2018**, *20*: 6932-6939; DOI: 10.1039/C8CE01389F.

[33] Zhang, H.; Nie, J.; Jiao, G.; Xu, X.; Yan, S.; Guo, X.; Zhang, T. Evolution of the Micropore Structure of Ammonium Perchlorate during Low-Temperature Decomposition and its Combustion Characteristics. *Appl. Sci.* **2021**, *11*: paper 9392; DOI: 10.3390/app11209392.

[34] Hori, K.; Iwama, A.; Fukuda, T. FTIR Spectroscopic Study on the Interaction between Ammonium Perchlorate and Bonding Agents. *Propellants Explos. Pyrotech*. **1990**, *15*(3): 99-102; DOI: 10.1002/prep.19900150307.

[35] Spassov, T.; Tzvetkov, G.; Lyutov, L. Novel Spherical Simonkolleite Nanoparticles and Their Promotional Effect on the Thermal Decomposition of Ammonium Perchlorate. *Vacuum* **2020**, *175*: paper 109285; DOI: 10.1016/j.vacuum.2020.109285.

[36] Yuan, Y.; Jiang, W.; Wang, Y.; Shen, P.; Li, F.; Li, P. Hydrothermal Preparation of Fe_2O_3/graphene Nanocomposite and Its Enhanced Catalytic Activity on the Thermal Decomposition of Ammonium Perchlorate. *Appl. Surf. Sci.* **2014**, *303*: 354-359; DOI: 10.1016/j.apsusc.2014.03.005.

[37] Jeremić, D.; Andjelković, L.; Milenković, M.R.; Šuljagić, M.; Šumar Ristović, M.; Ostojić, S.; Nikolić, A.S.; Vulić, P.; Brčeski, I.; Pavlović, V. One-Pot Combustion Synthesis of Nickel Oxide and Hematite: From Simple Coordination Compounds to High Purity Metal Oxide Nanoparticles. *Sci. Sinter.* **2020**, *52*(4): 481-490; DOI: 10.2298/SOS2004481J.

[38] Šumar Ristovic, M.; Minić, D.M.; Blagojević, V.; Andjelković, K. Kinetics of Multi-Step Processes of Thermal Degradation of Co(II) Complex with *N*-Benzyloxycarbonylglycinato Ligand. Deconvolution of DTG Curves. *Sci. Sinter.* **2014**, *46*(1): 37-53; DOI: 10.2298/SOS1401037S.

[39] Mahinroosta, M. Catalytic Effect of Commercial nano-CuO and nano-Fe_2O_3 on Thermal Decomposition of Ammonium Perchlorate. *J. Nanostructure Chem.* **2013**, *3*: paper 47; DOI: 10.1186/2193-8865-3-47.

[40] Cao, S.; Zhou, L.; Zhang, C.; Zhang, L.; Xiang, G.; Wang, J. Core-shell Structured AP/Fe_3O_4 Composite with Enhanced Catalytic Thermal Decomposition Property: Fabrication and Mechanism Study. *Chem. Eng. Sci*. **2022**, *247*: paper 116899; DOI: 10.1016/j.ces.2021.116899.

[41] Yang, F.; Pei, J.; Zhao, H. First-Principles Investigation of Graphene and Fe_2O_3 Catalytic Activity for Decomposition of Ammonium Perchlorate. *Langmuir* **2022**, *38*(12): 3844-3851; DOI: 10.1021/acs.langmuir.2c00027.

[42] Zhou, L.; Cao, S.; Zhang, L.; Xiang, G.; Wang, J.; Zeng, X.; Chen, J. Facet Effect of Co_3O_4 Nanocatalysts on the Catalytic Decomposition of Ammonium Perchlorate. *J. Hazard. Mater.* **2020**, *392*: paper 122358; DOI: 10.1016/j.jhazmat.2020.122358.

[43] Wang, J.; He, S.; Li, Z.; Jing, X.; Zhang, M.; Jiang, Z. Synthesis of Chrysalis-like CuO Nanocrystals and Their Catalytic Activity in the Thermal Decomposition of Ammonium Perchlorate. *J. Chem. Sci.* **2009**, *121*(6): 1077-1081; DOI: 10.1007/s12039-009-0122-8.

Received: September 21, 2022
Revised: June 14, 2023
First published online: June 30, 2023